Elastic Properties of Well-Defined, High-Density Poly(methyl methacrylate) Brushes Studied by Electromechanical Interferometry

Kenji Urayama,*,† Shinpei Yamamoto,† Yoshinobu Tsujii,† Takeshi Fukuda,† and Dieter Neher‡

Institute for Chemical Research, Kyoto University, Uji, Kyoto-fu 611-0011, Japan, and Institute of Physics, University of Potsdam, Am Neuen Palais 10, D-14469 Potsdam, Germany

Received May 28, 2002

ABSTRACT: We have investigated the elastic properties of dry polymer brushes comprising low-polydispersity poly(methyl methacrylate) (PMMA) chains with high graft densities over 0.4 chains/nm^2 by means of electromechanical interferometry. End-grafting on a glass plate by living radical polymerization yielded high-density brushes composed of the highly stretched graft chains, and the layer thickness of the brushes is 4−5 times as large as the unperturbed dimension of the graft chains. The layer thickness change induced by an applied electric field (electrostriction) is measured by a Nomarski optical interferometer as a function of temperature. The analysis of the electromechanical and dielectric data yields the plate compressibility (κ_p) of the brushes in the glassy and molten states. Comparison of the results for the high-density PMMA brushes and a reference spin-coated PMMA layer reveals the differences in the elastic and dielectric properties between a brush composed of highly stretched graft chains and a layer formed by the equivalent chains in the random-coiled state. The temperature dependence of the dielectric loss suggests that the glass transition temperature of the high-density brushes is ca. 10 °C higher than that of the spin-coat layer. In the glassy state, there is no appreciable difference in κ_p between the brushes and the spin-coat layer, whereas in the molten state, κ_p of the brushes is definitely (ca. 30−40%) lower than that of the spin-coated layer. This proves that the molten high-density PMMA brushes are more resistant against compression relative to the PMMA melt. The low compressibility of the molten high-density brushes is interpreted on the basis of rubber elasticity of entanglement network in the stretched state. This model successfully explains the magnitude of the plate compressibility of the brushes, which suggests that the low compressibility is mainly attributed to a strain-hardening effect of the highly stretched entanglement chains and that there exists a considerable amount of entanglements of different graft chains contributing to elastic modulus.

Introduction

Polymers terminally tethered (end-grafted) on a solid surface have attracted much attention of scientists and technologists because of their potential applications in colloidal stabilization, adhesion, lubrication, etc.[1−5] With increasing graft density, graft chains will be obliged to stretch away from the surface and form a so-called "polymer brush" due to small lateral spacings relative to the unperturbed coil dimensions.[6] Polymer brushes with high graft density as well as well-controlled chain length and its distribution have been prepared using living radical polymerization along with a high-efficiency initiator fixed on the substrate.[7−10] The graft densities of these high-density brushes are at least 1 order of magnitude larger than those of the earlier reported polymer brushes[11−19] prepared by the adsorption of block copolymers or end-functionalized polymers on a solid surface. The graft density of the polymer brushes made by the adsorption method is typically 0.001−0.05 chains/nm^2, and the swollen brushes in a good solvent are in the "moderately dense" regime in which graft chains overlap each other but the volume fraction of polymer chain in the layer is still low.

The surface properties of moderate-density polymer brushes swollen in a good solvent have been extensively investigated utilizing surface force apparatus (SFA),[11,12] atomic force microscopy (AFM),[13−16] and neutron reflectometry.[17−19] The AFM studies of the high-density poly(methyl methacrylate) (PMMA) brushes swollen in toluene have demonstrated that the graft chains are highly stretched relative to those of the moderately dense brushes prepared by the adsorption technique.[8,9] In addition, the longest brush studied was found to be compressible only to ca. 80% of the equilibrium layer thickness in the swollen state. The strong resistance against compression must be characteristic of the high-density brushes swollen by a good solvent. Meanwhile, their properties in the *dry* state are still to be disclosed.

For applications of grafted layers in ultrathin coating, the mechanical properties of the high-density brushes in the dry state are of special importance. Further, the investigation of the properties in the molten state at temperatures above the glass transition temperature (T_g) is an important issue with respect to existing theories to describe the viscoelasticity of polymers. Recently, Laup et al.[20] investigated the rheological properties of highly stretched molten polymer brushes as Langmuir monolayers at the air/water interface. They reported that the plateau modulus of the molten brushes is slightly smaller than or comparable to that of the bulk polymer under shear flow within the interface plane. However, to the authors' knowledge, there has been no experimental study on the mechanical properties, such as the plate compressibility, of high-density polymer brushes in the dry state, and the elasticity of the dry high-density brushes in the stretching direction of the graft chains has not yet been reported.

† Kyoto University.
‡ University of Potsdam.
* To whom correspondence should be addressed: e-mail urayama@scl.kyoto-u.ac.jp.

10.1021/ma0208279 CCC: $22.00
Published on Web 11/02/2002

In the present study, we investigate electrostrictive and dielectric properties of dry high-density PMMA brushes with well-controlled chain lengths and their distribution, prepared by the surface-initiated atom transfer radical polymerization technique, as a function of temperature by means of electromechanical interferometry and dielectric spectroscopy. It has been demonstrated that an optical interferometer based on the Nomarski principle is a powerful technique to investigate the electromechanical properties of thin polymer layers such as electrostriction and piezoelectricity.[21−26] Electrostriction is a function of the dielectric constant and the mechanical compliance, and hence the electrostrictive effect directly measured by the interferometer can be used to derive the plate compressibility, if the dielectric constant is known. The applied force acting on the brushes in the electromechanical measurement is compressive exclusively parallel to the stretching axis of the graft chains. In the present work, we compare the plate compressibility of the high-density PMMA brushes with that of a spin-coated layer of the equivalent free PMMA which was produced simultaneously with the graft PMMA chains. This comparison will clearly reveal possible differences in elastic properties between the polymer brushes comprising highly stretched chains and the polymer layer comprising randomly coiled chains.

Theoretical Background

We briefly describe here the theoretical background for the electromechanical interferometry employed in the present study. The details were given in our previous papers.[21−26] As described in the Experimental Section, the sample is a thin layer sandwiched between two metal electrodes. The sample configuration can be treated as a dielectric in a parallel plate capacitor. The thickness change Δh of the parallel plate capacitor induced by an applied electric field (E) is generally expressed as

$$\Delta h = h_0(1 + aE^2 + ...) \tag{1}$$

where h_0 is the layer thickness without external field and a is the electrostriction coefficient. Odd-order terms (due to inverse piezoelectric effect) are absent for the systems without net polarization as in the case of the layers used in the present study. An alternating electric field $E = E_0 \cos(\omega t)$ applied across the capacitor yields a periodic change in the layer thickness with double of the driving frequency ω

$$\frac{\Delta h}{h_0} = \frac{1}{2}aE_0^2 + \frac{1}{2}aE_0^2 \cos(2\omega t) + ... \tag{2}$$

In the experiment the field-induced thickness change $\Delta h(2\omega)$ modulated at 2ω is selectively measured by the frequency selective (lock-in) detection. The expression for a is derived from the consideration for the force between the electrodes using the Claussius−Musotti equation for $\partial\epsilon/\partial h$. This force yields a compression whose magnitude depends on the plate compressibility κ_p and dielectric constant ϵ of the material.

$$a(2\omega) = -\frac{\epsilon_0 k_p(2\omega)}{2}\left[\epsilon(\omega) + \frac{[\epsilon(\omega) + 2][\epsilon(\omega) - 1]}{3}\right] \tag{3}$$

From eq 3, κ_p is calculated if a and ϵ are measured. The plate compressibility κ_p is related to the shear modulus G or the Young's modulus E as

$$\kappa_p = \frac{(1 + \mu)(1 - 2\mu)}{(1 - \mu)E} = \frac{1 - 2\mu}{2(1 - \mu)G} \tag{4}$$

with Poisson's ratio μ. This relation is obtained by considering the sample geometry:[21] The horizontal expansion in the film plane by vertical compression is not possible because the layer is fixed onto the substrate.

Table 1. Sample Characteristics

sample	M_n (g/mol)	M_w/M_n	L_d[a] (nm)	graft density (chains/nm^2)	λ[b]
G1	214 000	1.21	125	0.42	4.7
G2	183 000	1.18	110	0.43	4.5
G3	104 000	1.21	75	0.52	4.1
G4	103 000	1.12	85	0.59	4.6
G5	106 000	1.16	75	0.51	4.0
SC1	106 000	1.16	110		
SC2	106 000	1.16	75		

[a] Layer thickness in the dry state [b] $\lambda = L_d/\langle R^2\rangle_\theta^{1/2}$, where $\langle R^2\rangle_\theta^{1/2}$ is the root of the mean-square end-to-end distance of the unperturbed free chain with the corresponding molecular weight.

Experimental Section

Sample Preparation. A bottom stripe electrode was prepared by vacuum-evaporating a 5 nm thick Cr layer and then a 100 nm thick Al layer through a mask on a cleaned glass plate. The Cr layer was used for the improvement of adhesion between the glass surface and the Al electrode layer. On top of the electrode-evaporated substrate, a ca. 10 nm thick SiO_x layer was deposited without a mask by a reactive evaporation of silicon monooxide in the presence of 10^{-4} Torr of oxygen. To immobilize the initiator, 2-(4-cholorosulfonylphenyl)ethyltrichlorosilane (CTCS) (Gelest, Inc., Morrisville, PA), this substrate was immersed in an anhydrous toluene solution of CTCS (ca. 1.0 wt %) for 2 h, washed with toluene, and then dried. The graft polymerization was carried out by the surface-initiated atom transfer radical polymerization (ATRP), as described previously.[7−10,27] In brief, the CTCS-fixed substrate was dipped in a degassed diphenyl ether solution of copper bromide (99.0% CuBr, 0.03 M), L-(−)-sparteine (0.06 M), methyl methacrylate (MMA, 5.0 M) and *p*-toluenesulfonyl chloride (TsCl, 5.0 mM) and heated for a prescribed period of time at 70 °C. TsCl was added as a free initiator to self-adjust the concentration of the Cu^{II} complex and thus to control the polymerization. After polymerization, the substrates were rinsed in a Soxhlet extractor with toluene for 12 h to remove physisorbed polymers.

Table 1 shows the characteristics of the samples. The number- and weight-average molecular weights (M_n and M_w) are the values as determined by PMMA-calibrated gel permeation chromatography (8020 high-speed liquid chromatograph, Tosoh Corp., Tokyo, Japan) for the free polymer chains which were simultaneously produced from the free (unbound) initiator added to the solution.[7−9,10a,27] There are reasons to believe that the molecular characteristics of the free polymers closely approximate those of the graft polymers.[7−9,10a,27] The reference spin-coated samples, SC1 and SC2, were prepared by spin-casting one of the free polymers from a chloroform solution on the same SiO_x-covered substrates as used for the grafted samples. Both the brushes and the spin-coated layers were annealed at 110 °C for 1 h. A top Al strip electrode with 50 nm thickness was deposited with an orientation perpendicular to that of the bottom strips. Thus, three independent and equivalent parallel plate capacitors (one of which is for reserve) with sandwich-type structure were constructed. The layer thickness L_d of the samples was measured by a Tencor α-step surface profiler. The graft density was calculated from M_n and L_d using the bulk density of a PMMA film (1.19 g/cm^3).[28] The

quantity λ in Table 1, which is a measure for the stretching degree of graft chains, is defined as the ratio of L_d to $\langle R^2\rangle_\theta^{1/2}$, the unperturbed mean-square end-to-end distance of the equivalent free chain. The value of L_d (and λ) of G4 is higher than those of G3 and G5 despite their comparable molecular weights, which may be attributable to the experimental errors (within 10%) involved in the estimations of L_d and M_n.

Dielectric Spectroscopy. Dielectric measurements were conducted at 4965 Hz just prior to the electromechanical measurements at each temperature using a home-built current/voltage amplifier in combination with a lock-in amplifier (Stanford Research Systems SR830). Frequency scanning dielectric measurements with the frequencies varying from 1 to 10^5 Hz were performed for the brush layer G5 and the spin-coated layer SC2 in temperature steps of ca. 10 °C from room temperature to 150 °C.

As described above, the PMMA layer is sandwiched together with 10 nm thick SiO_x layer between two Al electrodes. The dielectric properties of the PMMA layer from the total (measured) dielectric constant (ϵ_t) is derived as follows: Since the total electric capacitance C_t is given by $1/C_t = 1/C_p + 1/C_s$, where C_p and C_s are the electric capacitance of the polymer and SiO_x layer, respectively, the dielectric constant of the polymer layer ϵ_p is

$$\epsilon_p = \frac{\epsilon_t \epsilon_s h_p}{\epsilon_s h_t - \epsilon_t h_s} \tag{5}$$

where h_t, h_p, and h_s are the total thickness, the thickness of the polymer, and the thickness of the SiO_x layer, respectively. Using eq 5, ϵ_p (hereafter denoted as ϵ) was calculated from ϵ_t with $\epsilon_s = 3.8$.[29]

Electromechanical Interferometry. The details of the electromechanical interferometry and the setup were described elsewhere.[21−26] The interferometric technique is based on the Nomarski principle. Two orthogonally polarized He−Ne laser beams are reflected at each of the top Al electrodes of the probe and reference capacitors. An electric field applied only to the probe capacitor yields a phase shift (ϕ) between the two (probe and reference) reflected beams due to a field-induced thickness change (Δh) as $\phi = 4\pi\Delta h/\lambda$. The two reflected beams are recombined and split again by a Wallaston-type prism into two beams of perpendicular polarization with intensities A and B. At the working point of the interferometer, ϕ is proportional to the intensity difference ($A - B$). The modulation in $A - B$, i.e., ϕ, is measured directly utilizing a lock-in amplifier. The electrostriction measurements were performed at a modulation (detection) frequency $2\omega = 9930$ Hz, which is double the driving frequency (ω) of the applied ac voltage as shown in eq 2.

The effect of the thin SiO_x layer on the total (measured) electrostriction is considered in the following. The electric field acting on the polymer layer (E_p) is calculated using the boundary condition $D_p = D_s$ (i.e., $\epsilon_p E_p = \epsilon_s E_s$) as

$$E_p = \frac{U_0}{h_p + (\epsilon_p/\epsilon_s)h_s} \tag{6}$$

where U_0 is the total voltage between the two Al electrodes; D_p and D_s are the electric flux density for the polymer and SiO_x layer, respectively. Thus, the electrostriction constant of the polymer layer (a_p) is related to measured electrostiction constant (a_t) as

$$a_p = a_t\left(\frac{h_p}{h_t} + 2\frac{\epsilon_p h_s}{\epsilon_s h_t}\right) \tag{7}$$

where we assume that the electrostriction of the thin hard SiO_x layer is negligibly small relative to the electrostriction of the polymer layer, i.e., $\Delta h_s \ll \Delta h_p$, and the quadratic term in h_s is neglected due to the small magnitude ($h_s \ll h_p$). With eq 7, a_p (hereafter denoted as a) was computed from a_t.

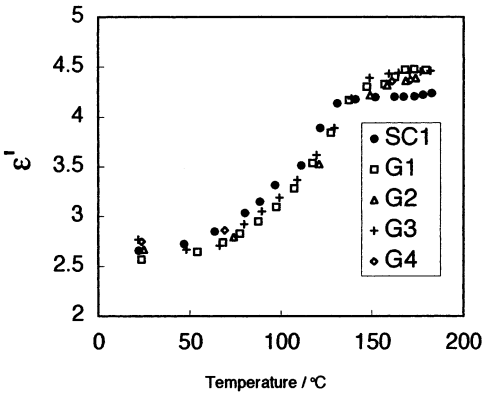

Figure 1. Temperature (T) dependence of real part of dielectric constant (ϵ') at 4965 Hz for the PMMA brushes G1−G4 and the spin-coated PMMA layer SC1.

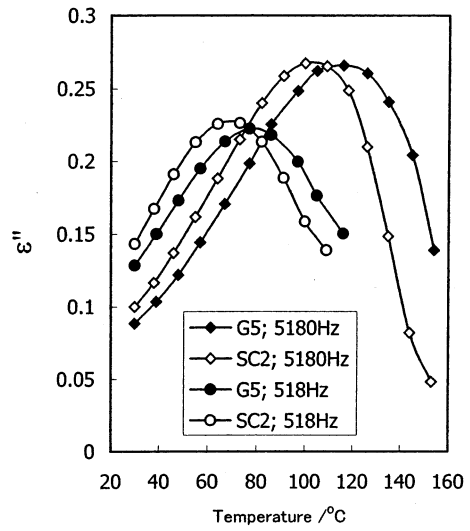

Figure 2. Temperature dependence of dielectric loss (ϵ'') at 5180 and 518 Hz for the PMMA brush G5 and the spin-coated PMMA layer SC2.

Results and Discussion

Dielectric Constant. Figure 1 shows the temperature (T) dependence of the real part of dielectric constant (ϵ') at 4965 Hz (corresponding to the driving frequency in the electromechanical measurements) for the high-density PMMA brushes G1−G4 and the PMMA spin-coated layer SC1. No significant difference in the absolute values of ϵ' over the whole temperature is observed between the different brushes as well as between the brushes and the spin-coated layer. The small variation is attributable to experimental error (within 10%) in layer thickness measurements. Since the dielectric constant is connected to the density of the polarizable units via the Clausius−Mosotti equation, this small variation suggests that all grafted layers have similar segmental densities and that the density is the same as in the spin-coated layer. With raising temperature, ϵ' increases due to softening around T_g and reaches the plateau value in the rubbery state.

Figure 2 illustrates the T dependence of the imaginary part of the dielectric constant (ϵ'') at 518 and 5180 Hz for the high-density brush G5 and the spin-coated layer SC2. At both frequencies, the maximum of ϵ'' for G5 appears at ca. 10 °C higher temperatures than for

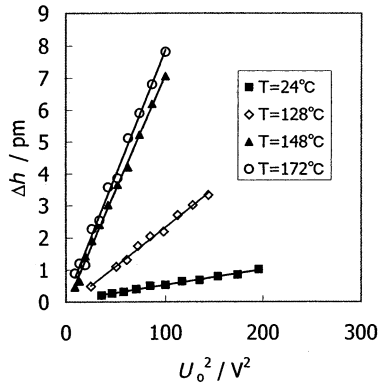

Figure 3. Field-induced layer thickness change (Δh) as a function of the square of the applied voltage (U_0) for the PMMA brush G1 at 27, 128, 148, and 172 °C. The modulation frequency is 9930 Hz.

SC2, while the absolute values of ϵ'' for G5 and SC2 are almost identical. The temperature of maximum ϵ'' is often employed as a measure of T_g.[30] This result suggests that T_g of the high-density PMMA brush is ca. 10 °C higher than that of the spin-coated PMMA layer.

For all other brushes G1−G4, the loss maximum (measured at 4965 Hz) appeared at almost the same temperature as that of G5 measured (at 5180 Hz). Also, the dielectric loss for the spin-coated film SC2 (at 4965 Hz) exhibited the maximum at the same position as for SC1 (at 5180 Hz) although the data are not presented here.) A similar result, namely a ca. 10 °C higher T_g of the high-density PMMA brushes relative to the reference spin-coated PMMA layers, has recently been obtained by thermal expansion measurements utilizing an optical ellipsometric technique.[31] The anisotropic structure of the graft layers as well as the presence of many anchoring points interacting with the substrate can yield differences in T_g between the brushes and the spin-coated layer.[31−34] The elipsometric measurement[31] revealed that, for the layers (whose thickness is over 70 nm) comprising relatively long graft chains such as investigated here, the higher T_g of the brushes is mainly due to the anisotropic structure rather than the interaction with the substrate. In fact, no appreciable change in T_g has been observed in earlier studies on low- to moderate-density brushes with 0.1 chains/nm^2 without developed anisotropic structure.[32,34] It should also be noted that our experiments on the brush and spin-coated layers are not affected by layer-thinning effects on T_g, since recent ellipsometric studies[31] proved that the layer-thinning effect are relevant only for layer thicknesses below ca. 50 nm.

Meanwhile, apart from a slight horizontal shift due to the difference in T_g, there is no significant difference in the dielectric loss spectra between G5 and SC2 which were obtained using the frequencies ranging from 1 to 10^5 Hz with varying the temperatures from 27 to 150 °C, although the data are not shown here: No appreciable dielectric relaxation specific to the high-density brush was observed.

Electrostriction. To obtain the T dependence of electrostriction constant a, voltage-scanning measurements of the electrostriction with the modulation frequency 9930 Hz (corresponding to a driving frequency of 4965 Hz) were carried out at different temperatures. In Figure 3, the field-induced thickness change Δh for the brush G1 at $T = 27$, 128, 148, and 172 °C is plotted against the square of the applied voltage (U_0). On the basis of the linear variation of Δh with U_0^2, the apparent electrostriction coefficient a_t (including the effect of the SiO_x layer) was evaluated by the least-squares method. The electrostriction coefficient a_p (a) of the polymer layer is calculated from a_t with eq 7.

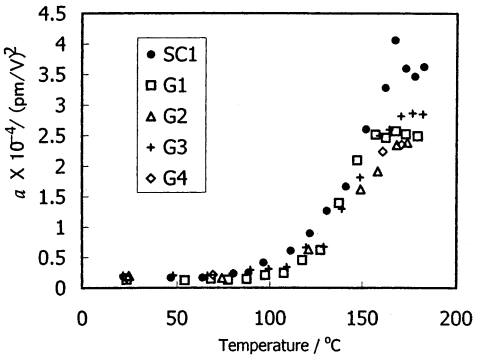

Figure 4. Electrostriction constant (a) as a function of temperature (T) for the PMMA brushes G1−G4 and the spin-coated PMMA layer SC1. The modulation frequency is 9930 Hz.

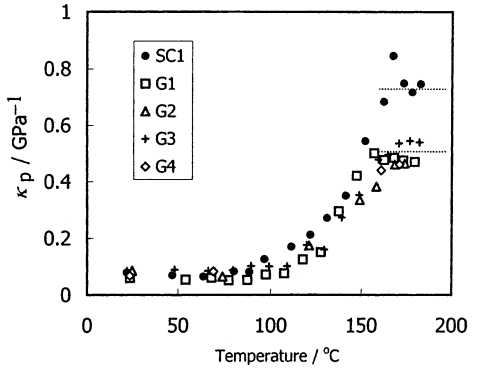

Figure 5. Plate compressibility (κ_p) as a function of temperature (T) for the PMMA brushes G1−G4 and the spin-coated PMMA layer SC1. The modulation frequency is 9930 Hz.

Figure 4 shows a for the high-density brushes G1−G4 and the spin-coated layer SC1 as a function of T. The value of a for each sample steeply increases with T due to the softening around T_g and eventually reaches a plateau value. It should be noticed that the T dependence of a for all the brushes examined here is almost identical. The small difference in the plateau values between the different brushes is mainly due to experimental error involved in the layer thickness determination. More interestingly, the plateau value of a in the molten state is significantly lower for the brushes than that for the spin-coated layer. It is found from eq 3 that the smaller a of the molten brushes primarily originates from the lower plate compressibility relative to the molten spin-coated layer, because the dielectric constants of the brushes and spin-coated layers are comparable (see Figure 1). Detailed comparison of κ_p for the brushes and the spin-coat layer is described below.

Plate Compressibility. Figure 5 illustrates plate compressibility κ_p for the high-density brushes and the spin-coated layer of PMMA as a function of T where κ_p is evaluated from eq 3 using the experimental values of ϵ' and a. A clear softening of each layer is observed around T_g. The result of κ_p for the 100 nm thick spin-coated layer obtained here is essentially the same as our previous result[21] for a 2.1 μm thick spin-coated PMMA film of $M_w = 101\,000$ without a thin SiO_x layer:

Each of the plateau values of κ_p in the glassy and molten states for the 2.1 μm thick spin-coated layer is ca. 0.1 and 0.8 GPa^{-1}, respectively, both of which are very close to the corresponding values for the 100 nm thick spin-coated layer investigated here. This good agreement ensures the absence of a layer-thinning effect on the magnitude of κ_p for the 100 nm thick spin-coated as well as the validity of the calibrations for ϵ and a using eqs 5 and 7.

All the PMMA brushes examined here exhibit almost the same T dependence of κ_p. Note that, unlike ϵ' and a values, the absolute value of κ_p is insensitive to experimental errors in layer thickness determination, because the effects of experimental error in layer thickness on ϵ' and a values almost cancel out in the calculation of κ_p (see eq 3). It appears that in the glassy region ($T < T_g$) κ_p of the brushes are not considerably different from that of the spin-coated layer, although the data in the glass state are relatively scattered which is due to the small electrostriction resulting from the low plate compressibility as well as the small layer thickness.

Most interestingly, κ_p in the rubbery region ($T > T_g$) for the high-density brushes is definitely smaller than that for the spin-coated layer: κ_p for the molten brushes corresponds to only ca. $^2/_3$ of that for the molten spin-coated layer. The difference in κ_p in the molten state between the brushes and spin-coated layer is undoubted: It is to be emphasized again that (1) both the brushes and spin-coated layer were composed of essentially the same PMMA on the same substrate, (2) they have almost the same layer thickness, and (3) the absolute value of κ_p is insensitive to experimental errors in layer thickness measurement as mentioned above. The lower values of κ_p in the molten state for the high-density brushes suggests that they are more resistant against compression than the PMMA melt.

An Interpretation of the Lower Plate Compressibility of the Molten High-Density Brushes. In this section, we try to interpret the strong resistance against compression observed for the molten high-density brushes. We assume here that the spin-coated layer and the brushes have the same Poisson's ratio (μ) in the molten state, because $\mu \approx {}^1/_2$ is reasonably assumed due to the imcompressibility.[21] This assumption and eq 4 allows us to discuss the difference in κ_p in terms of the difference in G.

In accounting for the high G (low κ_p) of the high-density brushes relative to the spin-coated layer, we have to consider the following two opposite effects of the highly stretched graft chains on elastic modulus: (1) the strain-hardening effect resulting from limited chain extensibility, which is often observed in stretching extensively cross-linked rubbers;[35,36] (2) the reduction in entanglement density due to a decrease in the overlapping degree of different graft chains, which is reasonably expected because the monomer densities of the molten PMMA brushes and the PMMA melt should be comparable. The reduction in entanglement density is roughly evaluated from the dimensional change of a single graft chain in the direction normal to stretching; i.e., $\alpha_T = R_{g,\perp}/R_{g0}$, where $R_{g,\perp}$ and R_{g0} is the gyration radius of the chain in the normal-to-stretch direction in the stretched and undeformed states, respectively. The difference in entanglement density should be proportional to α_T^2 because entanglement coupling results from binary interaction. The expression of $\alpha_T(\lambda)$ for a Gaussian chain whose end-to-end distance increases by a factor of λ was derived as $\alpha_T = [(\lambda + 1)/(2\lambda)]^{1/2}$.[37] This formula with $\lambda = 4-4.7$ (corresponding to the range of stretched ratio of the graft chains in the present study) yields $\alpha_T^2 = 0.59-0.61$, which expects that the entanglement density for the high-density brushes is ca. 40% lower than that for the polymer melt (the spin-coated layer). The former effect (1) and the latter one (2) yield the increase and decrease in elastic modulus, respectively. The experimental result of the lower κ_p of the high-density brushes implies that the former effect exceeds the latter one.

The elastic modulus of the polymer brushes can be theoretically evaluated, if the elastic free energy F_{el} is known. However, F_{el} for high-density brushes has not yet been derived due to the difficulties in considering the higher-order interaction as well as the limited chain extensibility. Instead, we argue here the elasticity of the molten high-density brushes on the basis of the analogy of rubber elasticity of a polymer entanglement network in the stretched state. The experimental fact that κ_p of the high-density brushes at 9930 Hz is independent of temperature in the molten state allows us to assume them as an entanglement network in the relevant time scale. The rubber elasticity of entanglement network can be theoretically described by the Edwards−Vilgis (E−V) slip-link model[38,39] in which entanglement is modeled as a fictitious mobile slip-link which attaches two entangled chains. The E−V slip-link model also considers the limited chain extensibility on the basis of the primitive path concept.[38,39] As a consequence, the slip-link model has the singularity in the chain entropy at the ultimate extension ratio λ_{max} given by $\lambda_{max} = n^{1/2}$, where n is the number of the Kuhn segments between adjacent entanglements.[38,39] The predictive ability of the E−V slip-link model for stress-elongation relation was experimentally confirmed by a multiaxial deformation study of an entanglement-dominated cross-linked rubbery network.[40] The slip-link model gives the true stress σ (force per deformed cross section) for entanglement network (without cross-links) under uniaxial deformation as[38,39]

$$\sigma/RT = \nu\left(\lambda^2 - \frac{1}{\lambda}\right)\left\{\frac{(1-\alpha^2)(1+\eta)}{A^2}\left[\frac{(1-\eta^2\lambda)\lambda^2 A}{B^2(\lambda+\eta)^2} + \alpha^2\left(\frac{\lambda^2}{B} + \frac{2}{\lambda+\eta}\right)\right] + \frac{\eta\lambda}{B(\lambda+\eta)} - \frac{\alpha^2}{A}\right\} \quad (8)$$

with $A = 1 - \alpha^2(\lambda^2 + 2/\lambda)$ and $B = 1 + \eta\lambda^2$, where R, ν, λ, and η are the gas constant, the number density of entanglement chains, the extension ratio, and a measure of the slippage of slip-links, respectively. ν is related to n by $\nu = \rho/(nm)$, where ρ and m are the polymer density and the molecular mass of a Kuhn segment, respectively. We use here $\eta = 0.2343$ proposed as a theoretical value.[41]

Equation 8 with $n = n_e = 29$ yields the stress-elongation relation of the PMMA entanglement network whose n is equivalent to the number of the Kuhn segments between adjacent entanglements for PMMA melt ($n_e = 29$).[42] Figure 6 illustrates the reduced stress as a function of λ for the entanglement network of $n = n_e$ where the stress is reduced by $3\nu_e RT$. The quantity ν_e is the entanglement density of PMMA melt given by $\nu_e = \rho/(n_e m)$, and the reduction factor $3\nu_e RT$ is equivalent to E or $3G$ ($E = 3G$ holds for incompressible material), where E is the Young's modulus. Note in Figure 6 that the initial slope (at $\lambda = 1$) for the

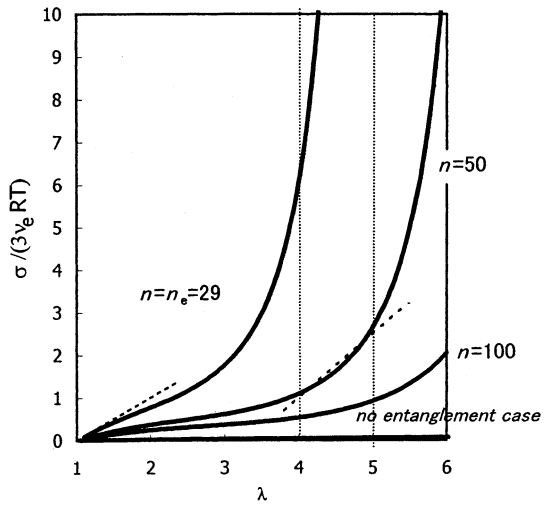

Figure 6. Reduced stress as a function of stretched ratio (λ) for the entanglement networks with $n = n_e$(=29), 50, and 100 on the basis of the slip-link model,[38,39] where n_e is the number of the Kuhn segments between adjacent entanglements in PMMA melt. The stress (σ) is reduced by $3\nu_e RT$, where ν_e is the entanglement density of PMMA melt. The dashed lines represent the tangents of the curves for $n = n_e$ at $\lambda = 1$ and for $n = 50$ at $\lambda = 4.3$, and the slopes of the lines are unity and ca. 1.5, respectively. The reduced stress-elongation curve in the case of no entanglement is also shown.

entanglement network of $n = n_e$, which is unity due to the reduction by $3\nu_e RT$, corresponds to E or $3G$ of the spin-coated layer. The strong upward curvature at high extensions is the direct consequence of the limited extensibility of the entanglement chains of $n = n_e$. It is to be noticed that in this figure the gradient at certain λ provides "small-strain" Young's modulus (E or $3G$) of a network stretched up to the corresponding λ. For the entanglement network of $n = n_e$, the gradient at $\lambda = 4.3$ (chosen as a typical stretched ratio of the graft chains in the present study) exceeds 10, which suggests that G of the nework of $n = n_e$ stretched up to $\lambda = 4.3$ is more than 1 order of magnitude larger than G of that in the undeformed state. This difference in G is too large to explain the difference in κ_p between the brushes and the spin-coated layer, which implies that the reduction in entanglement density for the brushes (i.e., $n > n_e$) must be considered.

As an opposite extreme case, i.e., no entanglement case, the reduced stress-elongation curve for $n = 300$ (corresponding to $M_n \approx 1 \times 10^5$ g/mol for a typical single graft chain in the present study) with the graft density $\gamma = 0.6$ chains/nm^2 is also illustrated in Figure 6. In this case, the total stress is simply given as a sum of the stress acting on a single graft chain. The stress is calculated on the basis of the classical non-Gaussian approach considering limited chain extensibility as $\sigma = \gamma kTn^{1/2}L^{-1}(\lambda/n^{1/2})$, where L^{-1} is the inverse Langevin function.[35] Evidently, the slope of the curve at $\lambda = 4-4.7$ is far below unity, which suggests that the magnitude of elastic modulus of the brushes cannot be explained in terms of the strain-hardening effect alone without considering the elastic contribution of a considerable amount of entanglement.

It can be seen in Figure 6 that if we assume $n = 50$, the gradient of the reduced stress-elongation curve at $\lambda = 4.3$ is ca. 1.5. This means that G of the entanglement network of $n = 50$ elongated up to $\lambda = 4.3$ is ca. $^3/_2$ times as large as G of the entanglement network of $n = n_e$ in the undeformed state. These characteristics of the entanglement network of $n = 50$ at $\lambda = 4.3$ apparently are in accord with the experimental results: κ_p of the polymer brushes with $\lambda = 4-4.7$ is ca. $^2/_3$ of κ_p of the spin-coated layer. In addition, the reduction in entanglement density for the brushes, $n_e/n = (29/50)$ obtained by this curve-fitting procedure, is close to the aforementioned evaluation $n_e/n \approx \alpha_T^2 = 0.59-0.61$. This good agreement for n_e/n may be viewed with some caution, because the equation for α_T employed here is for a Gaussian chain where the effect of limited chain extensibility on α_T is not considered. Nevertheless, the agreement should be considered reassuring in view of the roughness involved in these two independent approaches. Thus, the interpretation described here demonstrates that the low compressibility of the molten high-density brushes is mainly attributable to the strain hardening originating from the high stretching of the graft chains and that there exists a considerable amount of entanglement of different graft chains contributing to the elastic modulus.

Conclusions

The dielectric and electromechanical properties of dry PMMA brushes with high graft densities of more than 0.4 chains/nm^2 were studied as a function of temperature. The temperature dependence of the dielectric loss clearly indicates that T_g of the brushes is ca. 10 °C higher than that of corresponding spin-coated layers with comparable layer thickness. The higher T_g of the brushes is attributed to the anisotropic structure composed of the highly extended graft chains. In the molten state above T_g, the plate compressibility of the brushes is ca. 30−40% lower than that of a corresponding cast film. The magnitude of the plate compressibility of the brushes suggests that the strain-hardening effect by the highly stretched entanglement chains yields a larger resistance to compression. Our results and calculations further indicate a considerable entanglement between chains in the graft layers.

Acknowledgment. K.U. acknowledges financial support for the stay at Potsdam University by International Fellowship by the Ministry of Education, Science, Sports and Culture, Japan.

References and Notes

(1) Napper, D. H. *Polymer Stabilization of Colloidal Dispersions*; Academic Press: London, 1983.
(2) Raphaël, E.; de Gennes, P. G. *J. Phys. Chem.* **1992**, *96*, 4002.
(3) Klein, J. *Annu. Rev. Mater. Sci.* **1996**, *26*, 581.
(4) Klein, J.; Kumacheva, E. *Science*, **1995,** *269*, 816.
(5) Parnas, R. S.; Cohen, Y. *Rheol. Acta* **1994**, *33*, 485.
(6) de Gennes, P. G. *Macromolecules* **1980**, *13*, 1069.
(7) Ejaz, M.; Yamamoto, S.; Ohno, K.; Tsujii, Y.; Fukuda, T. *Macromolecules* **1998**, *31*, 5934.
(8) Yamamoto, S.; Ejaz, M.; Tsujii, Y.; Matsumoto, M.; Fukuda, T. *Macromolecules* **2000**, *33*, 5602.
(9) Yamamoto, S.; Ejaz, M.; Tsujii, Y.; Fukuda, T. *Macromolecules* **2000**, *33*, 5608.
(10) (a) Husseman, M.; Malmström, E. E.; McNamara, M.; Mate, M.; Mecerreyes, D.; Benoit, D. G.; Hedrick, J. L.; Mansky, P.; Huang, E.; Russell, T. P.; Hawker, C. J. *Macromolecules* **1999**, *32*, 1424. (b) Huang, X.; Wirth, M. J. *Macromolecules* **1999**, *32*, 1694. (c) Matyjaszewski, K.; Miller, P. J.; Shukla, N.; Immaraporn, B.; Gelman, A.; Luokala, B. B.; Siclovan, T. M.; Kickelbick, G.; Vallant, T.; Hoffmann, H.; Pakula, T. *Macromolecules* **1999**, *32*, 8716. (d) Zhao, B.; Brittain, W. J. *J. Am. Chem. Soc.* **1999**, *121*, 3557. (e) von Werne, T.; Patten, T. E. *J. Am. Chem. Soc.* **1999**, *121*, 7409. (f) Kim, J. B.; Bruening, M. L.; Baker, G. L. *J. Am. Chem. Soc.* **2000**, *122*, 7616.

(11) Taunton, H. J.; Toprakcioglu, C.; Fetters, L.; Klein, J. *Macromolecules* **1990**, *23*, 571.
(12) Watanabe, H.; Tirrell, M. *Macromolecules* **1993**, *26*, 6455.
(13) O'Shea, S. J.; Welland, M. E.; Rayment, T. *Langmuir* **1993**, *9*, 1826.
(14) Overney, R.; Leta, D.; Pictroski, C.; Rafailovich, M.; Liu, Y.; Quinn, J.; Sokolov, J.; Eisenberg, A.; Overney, G. *Phys. Rev. Lett.* **1996**, *76*, 1272.
(15) Courvoisier, A.; Isel, F.; François, J.; Maaloum, M. *Langmuir* **1998**, *14*, 3727.
(16) Kelly, T. W.; Schorr, P. A.; Johnson, K. D.; Tirrel, M.; Frisbie, C. D. *Macromolecules* **1998**, *31*, 4297.
(17) Cosgrove, T.; Heath, T. G.; Phipps, J. S.; Richardson, R. M. *Macromolecules* **1991**, *24*, 94.
(18) Levicky, R.; Koneripalli, N.; Tirrel, M.; Satija, S. K. *Macromolecules* **1998**, *31*, 3731.
(19) Anastassopoulos, D. L.; Vradis, A. A.; Toprakcioglu, C.; Smith, G. S.; Dai, L. *Macromolecules* **1998**, *31*, 9369.
(20) Luap, C.; Goedel, W. A. *Macromolecules* **2001**, *34*, 1343.
(21) Winkelhahn, H.-J.; Pakula, T.; Neher, D. *Macromolecules* **1996**, *29*, 6865.
(22) Levitus, M.; Glasser, G.; Neher, D.; Aramandia, P. F. *Chem. Phys. Lett.* **1997**, *277*, 118.
(23) Jaworek, T.; Neher, D.; Wegner, G.; Wieringa, R. H.; Schouten, A. J. *Science* **1998**, *279*, 57.
(24) Urayama, K.; Oliver, K.; Böhmer, R.; Neher, D. *J. Appl. Phys.* **1999**, *86*, 6367.
(25) Pralle, M. U.; Urayama, K.; Tew, G. N.; Neher, D.; Wegner, G.; Stupp, S. I. *Angew. Chem., Int. Ed.* **2000**, *39*, 1486.
(26) Urayama, K.; Tsuji, M.; Neher, D. *Macromolecules* **2000**, *33*, 8269.
(27) (a) Yamamoto, S.; Tsujii, Y.; Fukuda, T. *Macromolecules* **2000**, *33*, 5995. (b) Ejaz, M.; Ohno, K.; Tsujii, Y.; Fukuda, T. *Macromolecules* **2000**, *33*, 2870. (c) Ejaz, M.; Tsujii, Y.; Fukuda, T. *Polymer* **2001**, *42*, 6811. (d) Ejaz, M.; Yamamoto, S.; Tsujii, T.; Fukuda, T. *Macromolecules* **2002**, *35*, 1412. (e) Tsujii, Y.; Ejaz, M.; Yamamoto, S.; Fukuda, T.; Shigeto, K.; Mibu, K.; Shinjo, T. *Polymer* **2002**, *43*, 3837.
(28) Brandrup, J., Immergut, E. H., Eds. *Polymer Handbook*; John Wiley & Sons: New York, 1989.
(29) *Handbook of Chemistry and Physics*, 64th ed.; CRC Press: Boca Raton, FL, 1983.
(30) McCrum, N. G.; Read, B. E.; Williams, G. *Anelastic and Dielectric Effects in Polymeric Solids*, Dover Pub., Inc.: New York, 1991.
(31) Yamamoto, S.; Tsujii, Y.; Fukuda, T. *Macromolecules* **2002**, *35*, 6077.
(32) Prucker, O.; Christian, S.; Bock, H.; Ruehe, J.; Frank, C. W.; Knoll, W. *Macromol. Chem. Phys.* **1998**, *199*, 1435.
(33) Kawana, S.; Jones, R. A. L. *Phys. Rev. E* **2001**, *63*, 021501.
(34) Tate, R. S.; Fryer, D. S.; Pasqualini, S.; Montague, M.; de Pablo, J. J.; Nealey, P. F. *J. Chem. Phys.* **2001**, *115*, 9982.
(35) Treloar, L. R. G. *The Physics of Rubber Elasticity*, 3rd ed.; Oxford University Press: Oxford, 1975.
(36) Erman, B.; Mark, J. E. *Structures and Properties of Rubber-like Networks*; Oxford University Press: Oxford, 1997.
(37) Ullman, R. *J. Chem. Phys.* **1979**, *71*, 436.
(38) Edwards, S. F.; Vilgis, T. A. *Polymer* **1986**, *27*, 483.
(39) Edwards, S. F.; Vilgis, T. A. *Rep. Prog. Phys.* **1988**, *51*, 243.
(40) Urayama, K.; Kawamura, T.; Kohjiya, S. *Macromolecules* **2001**, *34*, 8261.
(41) Ball, R. C.; Doi, M.; Edwards, S. F.; Warner, M. *Polymer* **1981**, *22*, 1010.
(42) Ferry, J. D. *Viscoelastic Properties of Polymers*, 3rd ed.; Wiley: New York, 1980.

MA0208279